# Letters

## High-Frequency Injection Angle Self-Adjustment Based Online Position Error Suppression Method for Sensorless PMSM Drives

Guangdong Bi, Guoqiang Zhang, *Senior Member, IEEE*, Qiwei Wang, *Member, IEEE*, Dawei Ding, *Member, IEEE*, Binxing Li, Gaolin Wang, *Senior Member, IEEE*, and Dianguo Xu, *Fellow, IEEE*

***Abstract*—In the high-frequency (HF) signal injection based position sensorless permanent magnet synchronous motor (PMSM) drives, there is an estimated position error caused by the cross-saturation effect and other factors. In order to suppress the position error, an HF injection angle self-adjustment based online suppression method is proposed in this letter. By tracking the sign of the increment of the absolute back electromotive force in the estimated frame, the criterion of the HF injection angle self-adjustment can be determined online and the position error can be mitigated effectively. This method can avoid the offline measurement or the variation of the operating state, which has a satisfactory suppression effect for the position error under different operating conditions. The effectiveness is verified by experiments on a 2.2-kW PMSM drive platform.**

***Index Terms*—High-frequency (HF) signal injection, online suppression, permanent magnet synchronous motor (PMSM), self-adjustment.**

### I. Introduction

POSITION sensorless control schemes for permanent magnet synchronous motor (PMSM) have been widely investigated to improve the system robustness and reduce costs [1], [2]. High-frequency (HF) signal injection based method is an effective solution of zero- and low-speed operation for sensorless PMSM drives [3]. When adopting the HF signal injection method, there is an error in the estimated rotor position affected by the cross-saturation effect and other factors, which should be suppressed to improve the performance of sensorless drives [4].

It is an effective solution to mitigate the cross-saturation effect by optimizing the motor structure design. In [5], the inductance matrix from the finite element models was calculated and the rotor geometry was designed to reduce the estimation error caused by the cross-saturation effect. Since the design cost and the comprehensive performance indicators need to be considered, the control algorithm optimization based methods are alternative, including the offline measurement and the online detection methods.

Offline measurement methods mainly include the q-axis current factor, the finite-element analysis, and the lookup table. Generally, the cross-saturation effect will be more severe as the load becomes heavier. In [6], the estimated position error was compensated by utilizing the $q$-axis current factor obtained offline, which simplifies the implementation process but the measurement for different operating conditions is required. In [7], the properties of the cross-saturation inductance for different types of synchronous machines were described by finite-element analysis and the information was used to the position error compensation successfully. In [8], the saturation- induced saliencies were compensated effectively by using the structured neural network and the lookup table, which improves the sensorless control performance. Since the motor operating conditions are relatively complicated, the universality of the offline measurement methods is limited.

Online detection methods are investigated to overcome the limitations. In [9], the $d$–$q$ axis self-inductances and mutual inductances were identified online to calculate and compensate the position error, which depends on the accuracy of parameter identification. In [10], the position error was directly detected and compensated by varying the current vector angle, which has a good universality, but the detection accuracy is affected by the load variation. The impact was analyzed in depth in [11] and a current vector angle adaptive adjustment based method was presented to improve the suppression effect under different load conditions. The variation of the current vector angle may change the operating state of the motor and affect the sensorless control performance.

This letter proposes a HF injection angle self-adjustment based online position error suppression method for sensorless PMSM drives using the HF signal injection. By analyzing the relationship between the position error, the cross-saturation angle, and the injection angle, the impact of the cross-saturation

Manuscript received 25 July 2022; revised 29 August 2022; accepted 24 September 2022. Date of publication 28 September 2022; date of current version 18 November 2022. This work was supported in part by the Research Fund for the National Natural Science Foundation of China under Grant 52125701 and Grant 52177034 and in part by the Fundamental Research Funds for the Central Universities under Grant FRFCU5710092020. *(Corresponding author: Guoqiang Zhang.)*

The authors are with the School of Electrical Engineering and Automation, Harbin Institute of Technology, Harbin 150001, China (e-mail: bgd0309@163.com; zhgq@hit.edu.cn; wqw0543@163.com; dingdawei@hit.edu.cn; li_binxing@163.com; wgl818@hit.edu.cn; xudiang@hit.edu.cn).

Color versions of one or more figures in this article are available at https://doi.org/10.1109/TPEL.2022.3210105.

Digital Object Identifier 10.1109/TPEL.2022.3210105

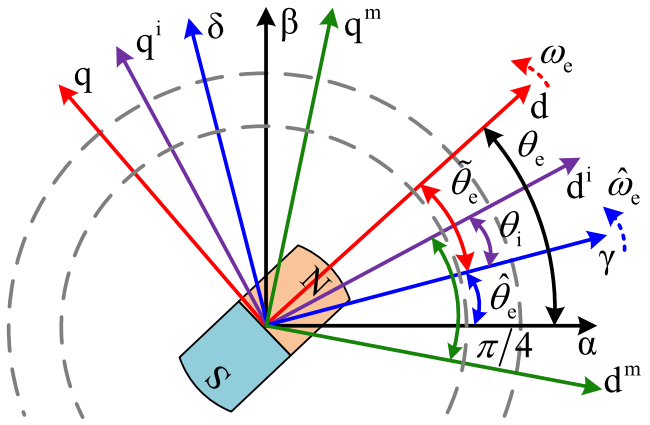


Fig. 1. Reference frames of PMSM.

effect can be mitigated by adjusting the injection angle. In order to determine the criterion of the injection angle self-adjustment, the sign of the increment of the absolute back electromotive force (EMF) in the estimated frame is analyzed and tracked online. The proposed method does not need to measure offline or change the operating state, which has a satisfactory suppression effect for the estimated position error. Finally, the experiments are implemented on a 2.2-kW PMSM drive platform to validate the effectiveness of this method.

## II. Proposed Position Error Suppression Method

### A. Rotor Position Error Considering Cross-Saturation Effect

The reference frames of PMSM are shown in Fig. 1. The $\alpha$–$\beta$, the $d$–$q$, the $\gamma$–$\delta$, the $d^i$–$q^i$, and the $d^m$–$q^m$ frames denote the stationary, the synchronous, the estimated, the injection, and the observation reference frames, respectively, where the $d^m$–$q^m$ frame lags the $d^i$–$q^i$ frame by 45°. $\omega_e$ and $\hat{\omega}_e$ are the actual and the estimated electrical angular speeds, respectively. $\theta_e$, $\hat{\theta}_e$, $\tilde{\theta}_e$, and $\theta_i$ are the actual rotor position, the estimated rotor position, the rotor position estimation error, and the HF injection angle, respectively.

Considering the cross-saturation effect, the HF mathematical model of PMSM in the $d^i$-$q^i$ frame can be expressed as

$$\begin{aligned}\begin{bmatrix} u_{dih} \\ u_{qih} \end{bmatrix} &= \boldsymbol{T}(\tilde{\theta}_e-\theta_i)\begin{bmatrix} L_{dh} & L_{dqh} \\ L_{qdh} & L_{qh} \end{bmatrix}\boldsymbol{T}^{-1}(\tilde{\theta}_e-\theta_i)\cdot\frac{\mathrm{d}}{\mathrm{d}t}\begin{bmatrix} i_{dih} \\ i_{qih} \end{bmatrix} \\ &= \begin{bmatrix} L_{mm} & L_{mn} \\ L_{nm} & L_{nn} \end{bmatrix}\cdot\frac{\mathrm{d}}{\mathrm{d}t}\begin{bmatrix} i_{dih} \\ i_{qih} \end{bmatrix} = \begin{bmatrix} (-1)^n U_i \\ 0 \end{bmatrix}\end{aligned} \tag{1}$$

where $u_{dih}$, $u_{qih}$, $i_{dih}$, and $i_{qih}$ are the $d^i$–$q^i$ axis HF voltages and currents, respectively, $U_i$ is the amplitude of the injected HF square-wave voltage, $L_{dh}$, $L_{qh}$, $L_{dqh}$, and $L_{qdh}$ are the $d$–$q$ axis self-inductances and mutual inductances, usually, $L_{dqh} = L_{qdh}$, $\boldsymbol{T}(\cdot)$ is the coordinate transformation matrix, $L_{mm}$, $L_{mn}$, $L_{nm}$, and $L_{nn}$ are the inductance coefficients, which can be expressed as

$$\begin{aligned}&\begin{bmatrix} L_{mm} \\ L_{mn} \\ L_{nm} \\ L_{nn} \end{bmatrix} \\ &= \begin{bmatrix} \Sigma L_h + \Delta L_h\cos(2\tilde{\theta}_e-2\theta_i) - L_{dqh}\sin(2\tilde{\theta}_e-2\theta_i) \\ \Delta L_h\sin(2\tilde{\theta}_e-2\theta_i) + L_{dqh}\cos(2\tilde{\theta}_e-2\theta_i) \\ \Delta L_h\sin(2\tilde{\theta}_e-2\theta_i) + L_{dqh}\cos(2\tilde{\theta}_e-2\theta_i) \\ \Sigma L_h - \Delta L_h\cos(2\tilde{\theta}_e-2\theta_i) + L_{dqh}\sin(2\tilde{\theta}_e-2\theta_i) \end{bmatrix}\end{aligned} \tag{2}$$

where $\Sigma L_h$ and $\Delta L_h$ denote the average and the difference inductances, which are defined as $\Sigma L_h = (L_{dh} + L_{qh})/2$ and $\Delta L_h = (L_{dh} - L_{qh})/2$.

According to (1) and (2), the $d^m$-$q^m$ axis HF currents are

$$\begin{aligned}\frac{\mathrm{d}}{\mathrm{d}t}\begin{bmatrix} i_{dmh} \\ i_{qmh} \end{bmatrix} &= \frac{(-1)^n U_i}{\sqrt{2}\left(L_{dh}L_{qh} - L_{dqh}^2\right)} \\ &\left\{\begin{bmatrix} \Sigma L_h \\ \Sigma L_h \end{bmatrix} + \left(\sqrt{\Delta L_h^2 + L_{dqh}^2}\right)\right. \\ &\left.\begin{bmatrix} \cos(2\tilde{\theta}_e+\theta_m-2\theta_i) - \sin(2\tilde{\theta}_e+\theta_m-2\theta_i) \\ \cos(2\tilde{\theta}_e+\theta_m-2\theta_i) + \sin(2\tilde{\theta}_e+\theta_m-2\theta_i) \end{bmatrix}\right\}\end{aligned} \tag{3}$$

where $i_{dmh}$ and $i_{qmh}$ are the $d^m$–$q^m$ axis HF currents and $\theta_m$ is the cross-saturation angle and $\theta_m = \tan^{-1}(-L_{dqh}/\Delta L_h)$.

Then, the equivalent position error signal can be expressed as

$$\begin{aligned}\varepsilon &= \mathrm{sign}\,(u_{dih})\cdot\left(2\tilde{\theta}_e+\theta_m-2\theta_i\right) \\ &\approx \frac{\left(L_{dh}L_{qh} - L_{dqh}^2\right)\frac{\mathrm{d}}{\mathrm{d}t}(i_{qmh}-i_{dmh})}{\sqrt{2}U_i\left(\sqrt{\Delta L_h^2 + L_{dqh}^2}\right)}.\end{aligned} \tag{4}$$

The equivalent position error signal can converge to zero by using a position observer, that is

$$\varepsilon = 0 \Leftrightarrow \tilde{\theta}_e = -\frac{1}{2}\theta_m + \theta_i. \tag{5}$$

According to (5), since the HF injection angle is usually 0° in the conventional method, there is an error of $-\theta_m/2$ in the estimated rotor position. The proposed method can track and adjust the injection angle online to offset the cross-saturation angle, i.e., $\theta_i \approx \theta_m/2$, as shown in Fig. 2. The HF square-wave voltage signal is injected into the $d^i$–$q^i$ frame and the induced HF current signal is processed in the $d^m$–$q^m$ frame. When the load condition changes, the HF injection angle starts to adjust automatically to suppress the estimated position error. The HF injection angle self-adjustment strategy is explained below.

### B. HF Injection Angle Self-Adjustment Strategy

Affected by the cross-saturation effect, $\theta_m$ will increase as the load becomes heavier. Theoretically, the position error can be eliminated when the HF injection angle is equal to $\theta_m/2$. However, it is difficult to obtain the value of $\theta_m$ online in the sensorless drive system. Hence, an effective self-adjustment criterion of HF injection angle needs to be established. In this

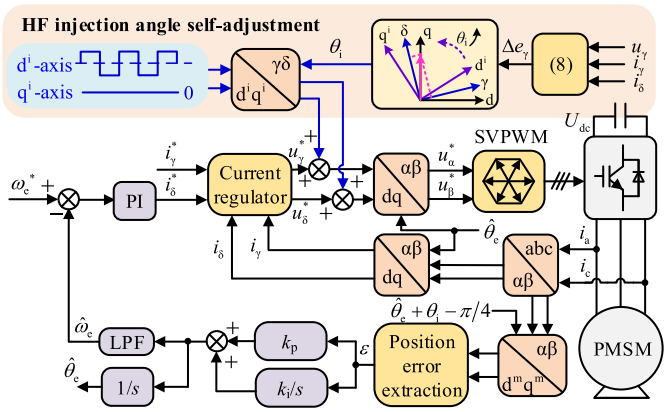


Fig. 2. Block diagram of the HF injection angle self-adjustment based online position error suppression method.

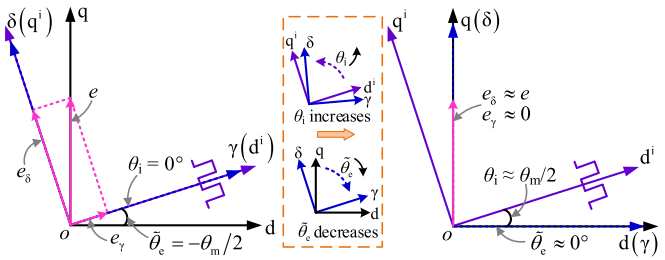


Fig. 3. Schematic diagram of HF injection angle self-adjustment.

letter, a $\gamma$-axis back EMF tracking based HF injection angle self-adjustment strategy is proposed. The detailed description is as follows.

Regardless of the HF injection signal, the back EMF in the $\gamma$–$\delta$ axis can be expressed as

$$\begin{aligned}\begin{bmatrix} e_\gamma \\ e_\delta \end{bmatrix} &= \begin{bmatrix} \omega_e\psi_f \sin\left(\frac{1}{2}\theta_m - \theta_i\right) \\ \omega_e\psi_f \cos\left(\frac{1}{2}\theta_m - \theta_i\right) \end{bmatrix} \\ &= \begin{bmatrix} u_\gamma - Ri_\gamma - L_d\frac{di_\gamma}{dt} + L_q\omega_e i_\delta \\ u_\delta - Ri_\delta - L_q\frac{di_\delta}{dt} - L_d\omega_e i_\gamma \end{bmatrix} \end{aligned} \tag{6}$$

where $\psi_f$ is the permanent magnet flux.

According to (6), the $\gamma$-axis back EMF is not equal to zero when the HF injection angle is 0°. Fig. 3 shows the schematic diagram of HF injection angle self-adjustment. It can be seen that the position error and $e_\gamma$ will decrease as the injection angle increases. Especially, when the HF injection angle is adjusted to about $\theta_m/2$, both the position error and $e_\gamma$ will converge to zero. Hence, the $\gamma$-axis back EMF can be used as the criterion of the injection angle self-adjustment, which can avoid the offline measurements.

According to (6), the calculation of the back EMF involves the inductances and resistance of the motor, the values of which may change under different load conditions. Then, $e_\gamma$ can be expressed as

$$\hat{e}_\gamma = u_\gamma - \hat{R}i_\gamma - \hat{L}_d\frac{di_\gamma}{dt} + \hat{L}_q\omega_e i_\delta \tag{7}$$

where $\hat{R}$, $\hat{L}_d$, and $\hat{L}_q$ are the resistance and the inductances under the corresponding operating condition, respectively.

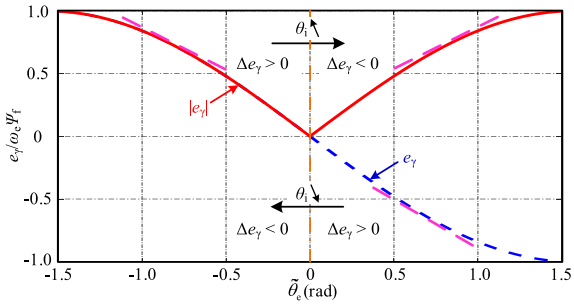


Fig. 4. Curves of per-unit $e_\gamma$ and $|e_\gamma|$ under different position error conditions.

Based on (7), there may be a calculation error in the $\gamma$-axis back EMF when the motor parameters change under heavy load conditions. In this letter, instead of the value of $e_\gamma$, the sign of the increment of the absolute $\gamma$-axis back EMF is tracked to judge the range of the HF injection angle self-adjustment, which can be expressed as

$$\begin{aligned}\Delta e_\gamma = |e_{\gamma 1}| - |e_{\gamma 2}| \approx &\left|u_{\gamma 1} - \hat{R}i_{\gamma 1} - \hat{L}_d\frac{di_{\gamma 1}}{dt} + \hat{L}_q\omega_e i_{\delta 1}\right| \\ &- \left|u_{\gamma 2} - \hat{R}i_{\gamma 2} - \hat{L}_d\frac{di_{\gamma 2}}{dt} + \hat{L}_q\omega_e i_{\delta 2}\right|\end{aligned} \tag{8}$$

where $\Delta e_\gamma$ is the increment of the absolute $\gamma$-axis back EMF, the subscripts "1" and "2" are the states of two adjacent high frequency injection angles, respectively.

According to (8), when the operating condition is constant, the motor parameters are approximately constant during the HF injection angle self-adjustment although they may be different from the nameplate values. Hence, the tracking of the sign of $\Delta e_\gamma$ may reduce the influence of motor parameters compared to the value of $e_\gamma$.

Fig. 4 shows the curves of per-unit $e_\gamma$ and $|e_\gamma|$ under different position error conditions. Since $e_\gamma$ is monotonic within a small error range, the sign of the increment of $e_\gamma$ will not change when the HF injection angle is adjusted so that the position error crosses zero. Since $|e_\gamma|$ is nonmonotonic, the sign of the increment of $|e_\gamma|$ can be used as the criterion of the HF injection angle self-adjustment, expressed as (9). The injection angle is adjusted continuously when $\Delta e_\gamma > 0$. Once $\Delta e_\gamma < 0$, the injection angle stops adjusting and maintains this value under this operating condition, realizing the online suppression of the estimated rotor position error

$$S_{\Delta e} = \begin{cases} 1, \Delta e_\gamma > 0 \\ -1, \Delta e_\gamma < 0 \end{cases}. \tag{9}$$

## III. Experimental Results

The proposed method was verified on a 2.2-kW PMSM experimental platform, as shown in Fig. 5. The rated speed, the rated current, the resistance, and the $d$–$q$ axis inductances are 1000 r/min, 5.6 A, 2.75 Ω, 35 mH, and 64 mH, respectively. The pulsewidth modulation (PWM) carrier frequency is set as 6 kHz. The injection frequency and amplitude are 750 Hz and 62

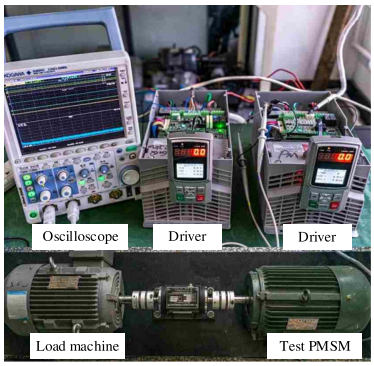


Fig. 5. Experimental platform with a 2.2-kW PMSM drive.

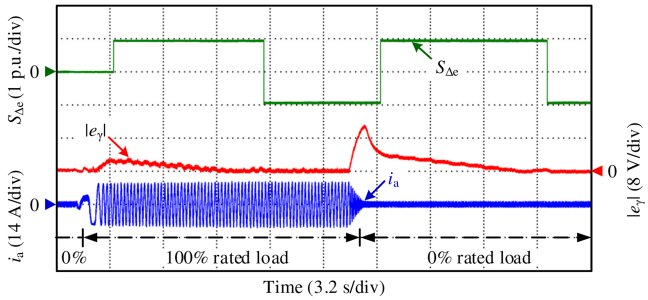


Fig. 6. Experimental results of $|e_\gamma|$ and $S_{\Delta e}$ under varying load conditions.

V, respectively. The experimental results using this method are as follows.

Fig. 6 shows the experimental results of $|e_\gamma|$ and $S_{\Delta e}$ using the proposed method under varying load conditions. Affected by the cross-saturation effect, there is an estimated position error and $\gamma$-axis back EMF under the 100% rated load disturbance condition. When $|e_\gamma|$ changes, the proposed method can track the sign of $|e_\gamma|$ accurately to determine the range of the HF injection angle self-adjustment, which is consistent with the analysis in (9). The injection angle is adjusted continuously when $S_{\Delta e}$ is positive and stops adjusting when $S_{\Delta e}$ is negative, verifying the feasibility of this method.

Fig. 7 shows the experimental results of position error suppression using the proposed method under the rated load disturbance and different speed conditions. In Fig. 7(a), when the load changes from 0% to 100%, the estimated position error is $-6.5°$. Then, the injection angle is adjusted from 0° and the position error decreases gradually in the self-adjustment region. When $S_{\Delta e} < 0$, the injection angle stops adjusting and maintains this value in the steady-state region. As a result, the position error is suppressed to 0.6° effectively. When the load changes back to 0%, the offset of the injection angle results in a positive position error, that is 7.1°. Then, the injection angle decreases automatically until $S_{\Delta e} < 0$ and the position error is reduced to $-0.9°$. When the operating speed is 60 r/min, as shown in Fig. 7(b), the position error can be suppressed to 0.4° and $-0.5°$ effectively. The experimental results are consistent with the analysis in Section II-B, verifying the effectiveness.

Fig. 8 shows the experimental results of position error suppression under different load conditions. In Fig. 8(a), when the

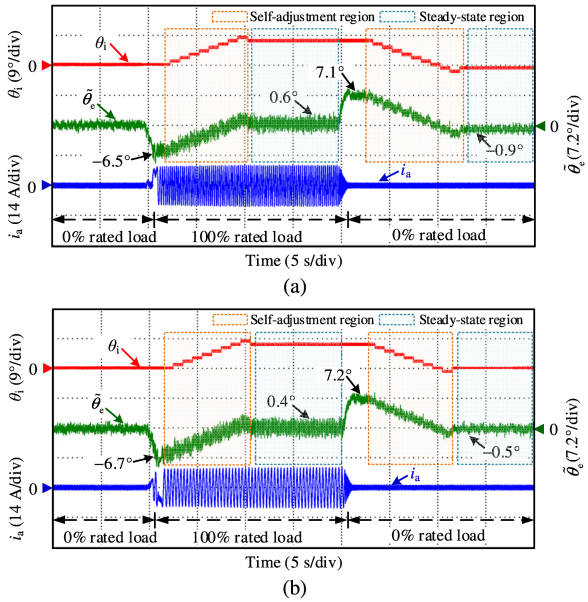


Fig. 7. Experimental results of position error suppression using the proposed method under the rated load disturbance conditions. (a) 100 r/min. (b) 60 r/min.

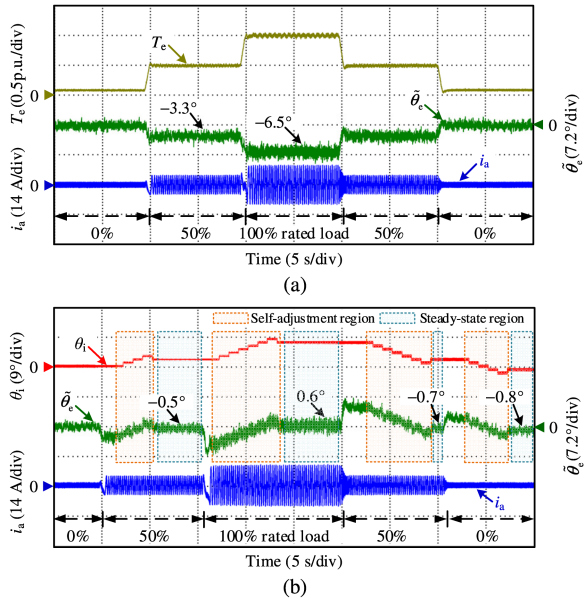


Fig. 8. Experimental results of position error suppression under different load conditions. (a) Without suppression method. (b) With the proposed method.

suppression method is not used, the estimated rotor position error is $-3.3°$ and $-6.5°$ under 50% and 100% rated load conditions, respectively. The experimental results indicate that the cross-saturation effect becomes more severe as the load becomes heavier. After using the proposed method, as shown in Fig. 8(b), the estimated position error is reduced to $-0.5°$, 0.6°, $-0.7°$, and $-0.8°$ when the load changes continuously between 0%, 50%, and 100%. It can be seen from the experimental results the HF injection angle is adjusted accurately and the position error is suppressed effectively.

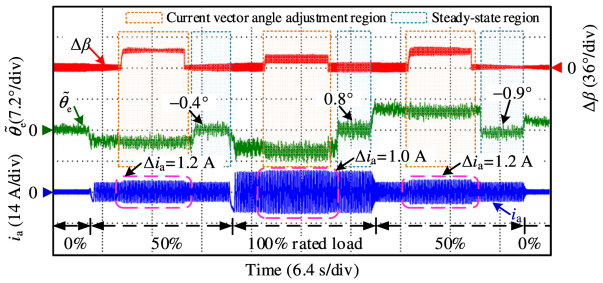


Fig. 9. Experimental results of position error suppression using the method investigated in [11].

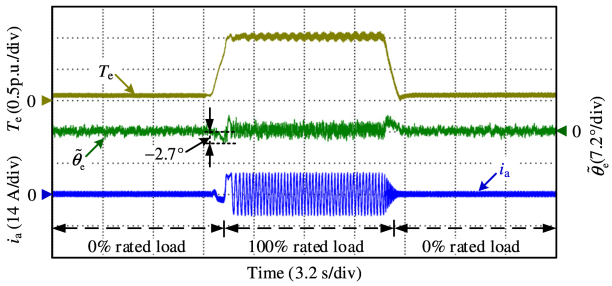


Fig. 10. Experimental results of position error suppression under transient-state conditions.

Fig. 9 shows the experimental results of position error suppression using the method investigated in [11] for a more intuitive comparison, where $\Delta\beta$ and $\Delta i_a$ are the variations of the current vector angle and the phase current amplitude during the process of position error detection, respectively. It can be seen that the position error can be suppressed effectively by adjusting the current vector angle adaptively. The amplitude of the phase current changes with the current vector angle during the process of position error detection, such as 1.2 A (21.4% of the rated current) at 50% rated load and 1.0 A (17.9% of the rated current) at 100% rated load, which may affect the normal operating state of the motor. In Fig. 8(b), when the proposed method is applied, the position error can also be suppressed effectively by adjusting the HF injection angle accurately and $\Delta i_a$ is always 0 A, which does not affect the normal operating state of the motor. The experimental results further verify the advantage of the proposed method.

Based on the principle of the position error suppression, both the proposed method and the method in [11] are effective under steady-state conditions. Although it is relatively difficult for these methods to suppress the position error directly during large torque transients, it is possible to suppress the transient-state position error by using the proposed method with a lookup table. Fig. 10 shows the experimental results of position error suppression under transient-state conditions. After using the lookup table, the transient-state position error is reduced to $-2.7°$ effectively under the 100% rated load disturbance condition, which further validates the possibility.

In order to further evaluate the sensorless control performance, the experimental results of the estimated and the actual rotor position under the 100% rated load condition are shown in Fig. 11. It can be seen that after using the proposed position error

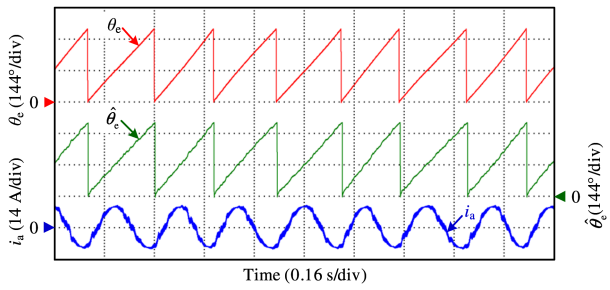


Fig. 11. Experimental results of the estimated and the actual rotor position under the 100% rated load condition.

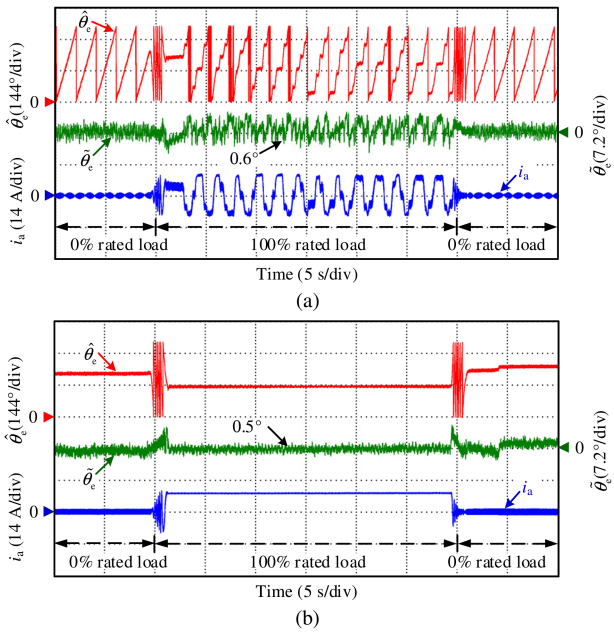


Fig. 12. Experimental results of sensorless operation at relatively low speeds. (a) Operating speed 10 r/min. (b) Operating speed 0 r/min.

suppression method, the motor can operate smoothly under the 100% rated load condition. Besides, the difference between the estimated and the actual rotor position is also relatively small.

Fig. 12 shows the experimental results of sensorless operation at relatively low speeds. It can be seen that the motor can operate stably at 10 and 0 r/min under 0% and 100% rated load conditions. When the operating speed is relatively low, the tracking accuracy of the back EMF may be decreased. Considering that the position error caused by the cross-saturation effect depends on the load and is independent of the speed, hence, the self-adjustment results of the HF injection angle obtained at the relatively high speed can be used for the position error suppression at the low speed. From Fig. 12, the position error at 10 and 0 r/min is suppressed effectively under the 100% rated load condition, which verifies the effect of sensorless operation and position error suppression at relatively low speeds.

When the HF signal injection method is applied, it will cause the HF losses and affect the operating efficiency inevitably. The HF losses mainly include and the copper loss and the iron loss, which are related to the injection amplitude and the injection frequency of HF signal, respectively. The iron losses mainly

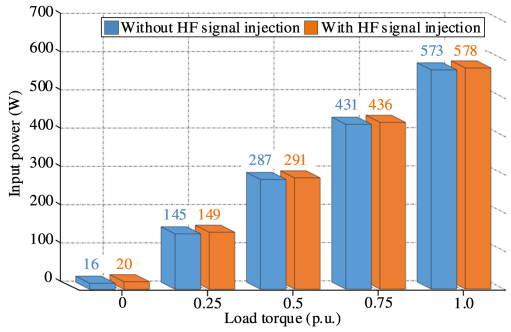


Fig. 13. Statistical measurement results of input power without and with HF signal injection method under different operating conditions.

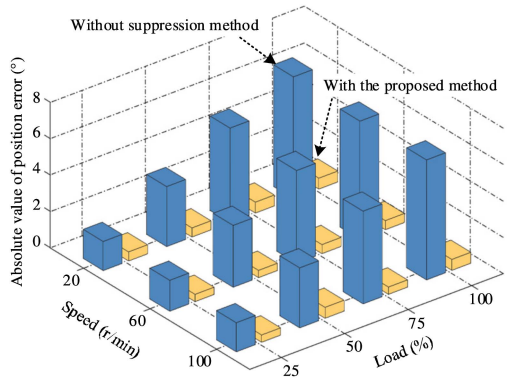


Fig. 14. Experimental comparison results of position error suppression under different operating conditions.

consist of the eddy current loss and the hysteresis loss [12]. In order to quantify the induced HF losses and the impact of the HF signal injection on the operating efficiency in the proposed method, the input power of the motor is measured and analyzed by using a precision power analyzer. The statistical measurement results under 250 r/min and different load conditions are shown in Fig. 13 . According to the measurement results, the HF losses in this method are approximately the same under different operating conditions. Specifically, after using the HF signal injection method, the operating efficiency is reduced by 0.9% under the 100% rated load condition. In order to ensure the sensorless control performance, the operating efficiency may be sacrificed slightly.

Fig. 14 shows the experimental comparison results of position error suppression under different speed and load conditions. It can be seen that the position error increases as the load becomes heavier and is independent of the speed. After using the proposed method, the position error under different operating conditions is suppressed effectively and its absolute value is kept within 1°.

## IV. Conclusion

As for the HF signal injection-based sensorless PMSM drive system, an HF injection angle self-adjustment-based online position error suppression method has been proposed in this letter. The proposed method can mitigate the impact of the cross-saturation effect on the estimation accuracy of the rotor position by adjusting the HF injection angle automatically. The sign of the increment of the absolute $\gamma$-axis back EMF can be tracked accurately to determine the range of the HF injection angle self-adjustment. This method does not need to measure offline or change the operating state, which has a satisfactory suppression effect for the position error under different load conditions. The absolute value of the position error can be suppressed within 1° effectively.

## References

[1] G. Wang, R. Yang, and D. Xu, "DSP-based control of sensorless IPMSM drives for wide-speed range operation," *IEEE Trans. Ind. Electron.*, vol. 60, no. 2, pp. 720–727, Feb. 2013.

[2] D. Xiao et al., "Universal full-speed sensorless control scheme for interior permanent magnet synchronous motors," *IEEE Trans. Power Electron.*, vol. 36, no. 4, pp. 4723–4737, Apr. 2021.

[3] G. Wang, R. Liu, N. Zhao, D. Ding, and D. Xu, "Enhanced linear ADRC strategy for HF pulse voltage signal injection-based sensorless IPMSM drives," *IEEE Trans. Power Electron.*, vol. 34, no. 1, pp. 514–525, Jan. 2019.

[4] J. Lee, Y. Kwon, and S. Sul, "Signal-injection sensorless control with tilted current reference for heavily saturated IPMSMs," *IEEE Trans. Power Electron.*, vol. 35, no. 11, pp. 12100–12109, Nov. 2020.

[5] P. Sergeant, F. Belie, and J. Melkebeek, "Rotor geometry design of interior PMSMs with and without flux barriers for more accurate sensorless control," *IEEE Trans. Ind. Electron.*, vol. 59, no. 6, pp. 2457–2465, Jun. 2012.

[6] J. M. Liu and Z. Q. Zhu, "Novel sensorless control strategy with injection of high-frequency pulsating carrier signal into stationary reference frame," *IEEE Trans. Ind. Appl.*, vol. 50, no. 4, pp. 2574–2583, Jul./Aug. 2014.

[7] D. Mingardi, M. Morandin, S. Bolognani, and N. Bianchi, "On the proprieties of the differential cross-saturation inductance in synchronous machines," *IEEE Trans. Ind. Appl.*, vol. 53, no. 2, pp. 991–1000, Mar./Apr. 2017.

[8] P. García, F. Briz, D. Raca, and R. D. Lorenz, "Saliency-tracking-based sensorless control of AC machines using structured neural networks," *IEEE Trans. Ind. Appl.*, vol. 43, no. 1, pp. 77–86, Jan./Feb. 2007.

[9] Q. Tang, A. Shen, X. Luo, and J. Xu, "PMSM sensorless control by injecting HF pulsating carrier signal into ABC frame," *IEEE Trans. Power Electron.*, vol. 32, no. 5, pp. 3767–3776, May 2017.

[10] H. Wang, K. Lu, D. Wang, and F. Blaabjerg, "Simple and effective online position error compensation method for sensorless SPMSM drives," *IEEE Trans. Ind. Appl.*, vol. 56, no. 2, pp. 1475–1484, Mar./Apr. 2020.

[11] G. Bi, N. Zhao, G. Zhang, R. Jing, G. Wang, and D. Xu, "Current vector angle adaptive adjustment based rotor position offset error suppression method for sensorless PMSM drives," *IEEE Trans. Power Electron.*, vol. 36, no. 9, pp. 10536–10547, Sep. 2021.

[12] S. Yang and R. D. Lorenz, "Analysis of iron and magnet losses in surface-permanent-magnet machines resulting from injection-based self-sensing position estimation," *IEEE Trans. Ind. Appl.*, vol. 48, no. 6, pp. 1901–1910, Nov./Dec. 2012.